CO_2 Capture using a novel hybrid monolith (H-ZSM5/Activated carbon) as adsorbent by combined Vacuum and Electric Swing Adsorption (VESA)

Qinghu Zhao[1], Fan Wu[1], Yuhan Men[1], Xin Fang[1], Jianhua Zhao[1], Penny Xiao[1,*], Paul A. Webley[1,*] and Carlos A. Grande[2]

[1]Department of Chemical Engineering, the University of Melbourne, VIC 3010, Australia

[2] SINTEF Industry, P.O. Box 124 Blindern, N0314 Oslo, Norway

Abstract:

Electrical Swing Adsorption (ESA) is an interesting cyclic adsorption technology which relies on rapid Joule heating of the adsorbent to liberate adsorbed molecules such as CO_2. In this study we used a novel hybrid zeolite/activated carbon honeycomb to implement ESA and compared it to conventional vacuum swing adsorption (VSA) for CO_2 capture. We then combined electrical and vacuum swing adsorption (VESA) to assess the merits of this dual regeneration technology for recovering CO_2 from a 15% CO_2/N_2 gas stream at low pressure. With a simple VSA-only cycle, a CO_2 downstream purity of only 17 to 23 % was achievable when the desorption pressures varied from 30 to 10 kPa. This was primarily due to the adsorbent's poor adsorption characteristics which provided little change in CO_2 adsorption capacity over this pressure range. A CO_2 product purity of 15 to 34% and a recovery of 29 to 78% was achieved with ESA as the electrification time was extended from 30 s to 180 s. The combined VESA process provided a CO_2 purity of 33% and recovery of 72% with a short electrification time of 30s at a mild desorption pressure of 10kPa. Energy

calculations indicate that the total specific energy for VESA was lower than ESA alone but still higher than VSA, although the latter suffered from low purity.

Keywords: *CO2 capture, hybrid monolith (H-ZSM5/Activated carbon), Vacuum and Electric Swing Adsorption (VESA)*

1. Introduction

Adsorption technology is a promising carbon capture option for specific applications. Vacuum Swing Adsorption (VSA) is the most researched adsorption technique for CO_2 capture from flue gas, since the inlet gas is available at atmospheric pressure and desorption at sub-atmospheric pressure is preferable to compression of the feed stream [1]–[4]. In the VSA process, desorption of the CO_2 often requires very deep vacuum to achieve high CO_2 purity since the majority of the adsorption of CO_2 occurs between 0 and 1 atm [4], [5]. Deep vacuum pressure results in relatively high energy consumption, not to mention the very large, low pressure gas flows and associated pressure drop problems. Higher throughput and lower specific power consumption are essential in order to enhance process economics for adsorption processes.

The adsorption capacity of CO_2 decreases as temperature increases [6]. Thus, vacuum desorption operated with simultaneous temperature swing (Vacuum Temperature Swing Adsorption) should improve the amount of CO_2 desorbed. Wang *et al.* studied vacuum temperature swing adsorption process (VTSA) for CO_2 capture from post-combustion flue gas and concluded that the regeneration conditions of VTSA process were much gentler than that of TSA or VSA and the energy consumption was lower than both of the single methods [7]. Plaza *et al.* also compared the performance of VSA, TSA and VTSA for CO_2 capture using activated carbon as adsorbent. In their experiments, CO_2 productivity and recovery followed the sequence VTSA > VSA > TSA and a productivity of 1.9 mol kg^{-1} h^{-1} and a CO_2 recovery up to

97% was achieved under VTSA operation [8]. Su *et al.* studied VTSA for CO_2 capture using amine-modified carbon nanotubes and achieved relatively higher desorbed CO_2 concentrations even in the presence of saturated water vapor [9]. These results suggest that VTSA has the potential to be a promising CO_2 capture technology, relying on synergies between temperature and pressure to help reduce overall energy demand. However, conventional TSA suffers from long heating time when heating the solid adsorbent by passing a hot gas through the adsorption column. This leads to a corresponding lower bed productivity.

Electric Swing Adsorption (ESA) has recently attracted some attention due to its higher regeneration efficiency, and shorter heating time [10]–[13]. In the desorption process of ESA, heat is generated in-situ by the Joule Effect achieved by passing electrical current through a conductor which is either the adsorbent or is directly adjacent to the adsorbent [14]. Compared with conventional TSA, ESA offers a much faster regeneration step which shortens the overall cycle time [15]. This increases adsorbent productivity and produces high product purity and recovery [14]. However, the inert gas employed to purge CO_2 from the adsorbent in the ESA regeneration process has a negative impact on CO_2 product purity [10], [11]. CO_2 purity dilution by inert gas in the regeneration step can be avoided with vacuum desorption since CO_2 partial pressure gradient is the driving force for CO_2 desorption and can be achieved by either concentration reduction (a purge) or total pressure reduction (vacuum). Therefore, the combination technology of ESA and VSA (VESA), that is raising the temperature of adsorption bed by alternative Joule heat and evacuating CO_2 with vacuum pressures, could potentially improve CO_2 capture performance and reduce energy consumption.

In conventional ESA work, activated carbon is the most common adsorbent because of its good electrical conductivity, easy availability, and low cost. In our previous ESA studies [15], activated carbon monolith was employed as the adsorbent, and the impact of operating parameters on CO_2 capture performance was studied [16]. Compared with zeolites, activated carbon shows a relatively low CO_2 adsorption capacity and low CO_2/N_2 selectivity, particularly in the range of low pressures [17], [18]. Our research partner - Corning European Technology Centre (CETC, France) - through the MATESA project developed a series of novel honeycomb monoliths, in which ZSM-5 and activated carbon were mixed evenly, to improve CO2 adsorption characteristics and grant electrical conductivity. Equilibrium adsorption for CO_2 and N_2 and electric conductivity for the monolith sample were measured and are presented in this paper. The working capacity of CO_2 and selectivity of CO_2/N_2 on this adsorbent at various regeneration temperatures and desorption pressures was also calculated and analysed. Using the novel hybrid monolith as adsorbent, VSA, ESA and VESA processes with simple cyclic steps were conducted to investigate the impact of each processing parameter on the separation performance for CO_2 capture from simulated flue gas streams. Energy consumption for CO_2 capture via VESA, ESA and VSA processes were also analysed and compared.

2. Materials

2.1. Physical properties and adsorption capacities of the honeycomb monolith

The hybrid honeycomb monoliths (Fig.1) were provided by Corning European Technology Centre (CETC, France). They were prepared using NH4-ZSM-5 (Zeolyst, The Netherlands with SiO_2/Al_2O_3 = 30) and phenolic resin (Veritas House, Mumbai,

India). The mixture was extruded, dries and then heated to convert the resin into carbon [19]. The resulting zeolite content in the final sample is approx. 82%. The physical properties of the samples are provided in Table 1.

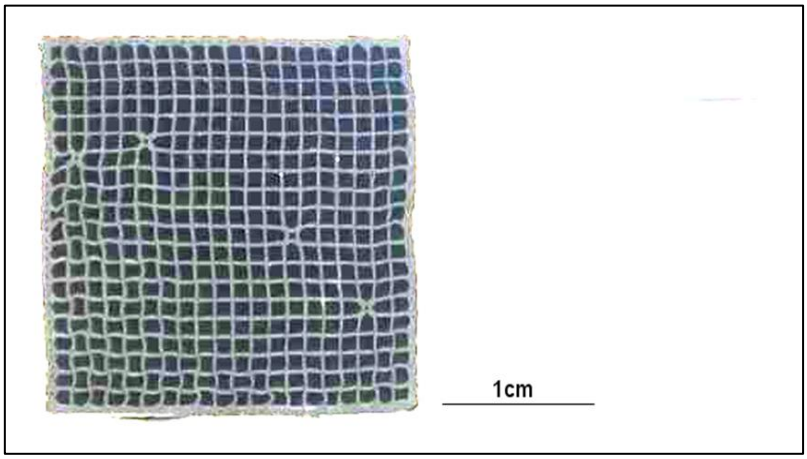

Fig.1: Cross section of hybrid honeycomb monolith

Table. 1: Physical properties of the honeycomb monolith

Wall density	**ρ**	kg/m^3	1440*
Resistance	R	**Ω**	403.33-0.7947T_s
Heat capacity	C_p	J/(kg·K)	5.3T_s-636.8*
Length	l	cm	23
Width	d	cm	2.5
Cell density	CPI	1	400
Channel width	l_{ch}	mm	0.9
Wall thickness	w	mm	0.3

*****[19]

Equilibrium adsorption of CO_2 and N_2 on the monolith was measured with a gas sorption analyser (ASAP2010, Micromeritics, US) at the temperatures of 273.15 K, 293.15 K, 323.15 K and 373.15 K and are shown in Fig.2 and the Dual-site Langmuir Model parameters which fit the experimental data are provided in Table 2. Each

sample was degassed under vacuum at the temperature of 350 °C for 6 hours to remove the adsorbed impurities (i.e., CO_2, H_2O) prior to adsorption measurements.

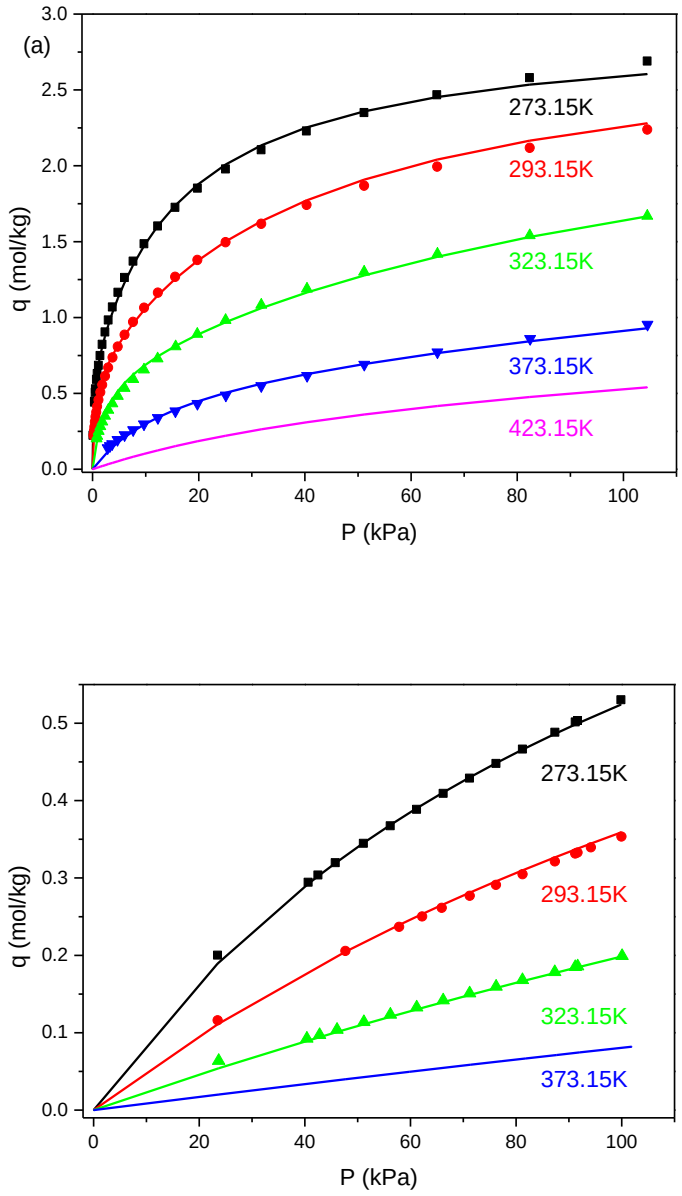

Fig. 2: Isotherms of CO_2 (a) and N_2 (b) on the hybrid monolith at the temperatures of 273.15 K (black), 293.15 K (red), 323.15 K (green), 373.15 K (blue) and 423.15 K (magenta); symbols – experimental data and lines – fitted Dual-site Langmuir model

Table.2: Dual-site Langmuir model parameters

	M_1 (mol/kg)	B_1 (1/kPa)	Q_1 (J/mol)	M_2 (mol/kg)	B_2 (1/kPa)	Q_2 (J/mol)
CO_2	0.6435	4.50×10^{-7}	-36967	2.272	1.30×10^{-7}	-29630
N_2	1.1479	1.04×10^{-6}	-20437	-	-	-

$$q(T,P) = M_1 \frac{B_1 \exp\left(-\frac{Q_1}{RT}\right)P}{1 + B_1 \exp\left(-\frac{Q_1}{RT}\right)P} + M_2 \frac{B_2 \exp\left(-\frac{Q_2}{RT}\right)P}{1 + B_2 \exp\left(-\frac{Q_2}{RT}\right)P} \qquad (1)$$

where q(T, P) is the loading (mol/kg) at temperature T (K) and pressure P (kPa), M_1 and M_2 represent saturated adsorption amounts corresponding to site I and site II, B_1 and B_2 are adsorption coefficients (1/kPa), Q_1 and Q_2 are adsorption heats on sites I and II (J/mol), R is the universal gas constant (8.3145 J/(mol·K)).

2.2. Electrical resistance of the monolith at various temperatures

The electrical resistance (R) of the hybrid monolith in the temperature range of 30 to 120 °C was measured and can be described by the following equation [20]:

$$R(T) = R_r + \alpha_r(T - T_r) \qquad (2)$$

Where, $T_r$and R_r are reference temperature and resistance respectively.

The electric resistance declined linearly as the temperature increased. From our measurements, $T_r = 306$ K, $R_r = 160.15\ \Omega$ and $\alpha_r = -0.7947\ \Omega/\mathrm{K}$ were obtained by a linear regression with $R^2 = 0.984$.

3. Experimental Work

3.1. Experimental setup

As shown in Fig. 4, the experimental apparatus for adsorption process work can be divided into three parts: adsorption column, gas system and measurement instruments. The square hybrid honeycomb monolith was placed into a steel column and two copper sheet electrodes (with length of 10 cm, width of 2.5 cm and thickness of 0.02 cm) were attached to each end of the monolith, with silver paint (SPI, US) applied to the contact area to increase conductivity. The electrodes were further immobilized with silicon tape. Finally, the whole monolith was covered with PTFE (Teflon) tape to avoid gas leakage through the porous walls, and to isolate the monolith from the steel column to prevent electrical short circuits. A constant voltage power source (HCS-3303, Manson, China) supplied from 0 – 60.5 V was employed to generate heat in the monolith. The whole adsorption column was covered with glass fibre and rubber to insulate it from the environment to minimise heat loss. Feed gas and N_2 purge gas were maintained with a mass flow controller (MFC) (Brooks, US) and exhaust gas was measured with a mass flowmeter (MF) (Brooks, US). A pressure regulator was located in the inlet line to control feed gas pressure. Pressure in the system was measured with a pressure transducer (PT). Temperature change at the surface of the monolith was monitored with a T-type thermocouple which was attached onto the monolith surface in the adsorption column. Real time CO_2 concentrations for both exhaust and desorption gases were analysed with an IR1520 Infrared Transducer (Servomex, US). Experimental data from MFC, MF, T and PT were acquired and recorded with LabVIEW software. A vacuum pump (XDS-10, Brooks) was used to evacuate the desorbed gas from the adsorption column during VSA and VESA experiments.

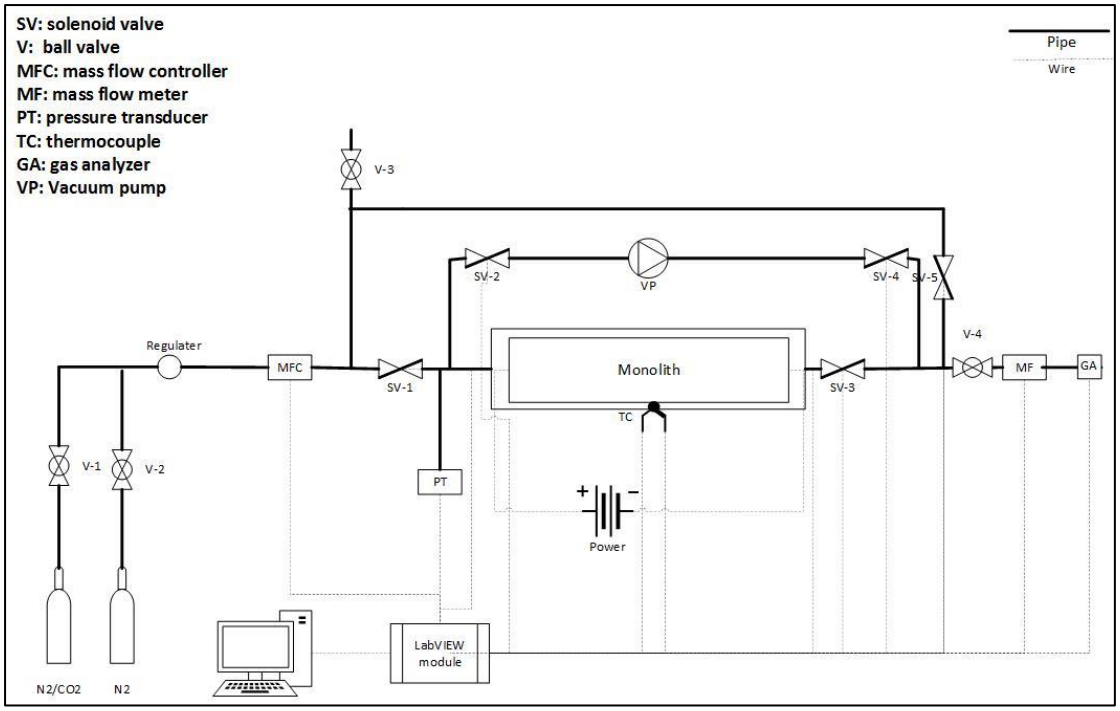

Fig.3: Schematic diagram of ESA system

Breakthrough experiments, VSA, ESA and VESA cyclic experiments were all conducted using this apparatus. All adsorption experiments were conducted with a feed gas of 15% CO_2 and 85% N_2, a feed temperature of 295 K, a pressure of 103 kPa and a flowrate of 1200 ml/min. Different steps for the three adsorption technologies were programmed in the LabVIEW software and achieved by opening/closing appropriate valves in the system.

3.2. Breakthrough experiments

To quantify the mass transfer in the monolith, breakthrough experiments were conducted. Feed gas of 15% CO_2 in N_2 was introduced into the feed end of the column and eluted from the product. This breakthrough curve was analysed and compared with that using commercial activated carbon monolith (MAST, UK) as conducted in our previous work [16].

3.3. VSA experiments

A simple cyclic VSA experiment, containing adsorption, vacuum desorption and re-pressurisation, was employed, as shown in Fig.4a.

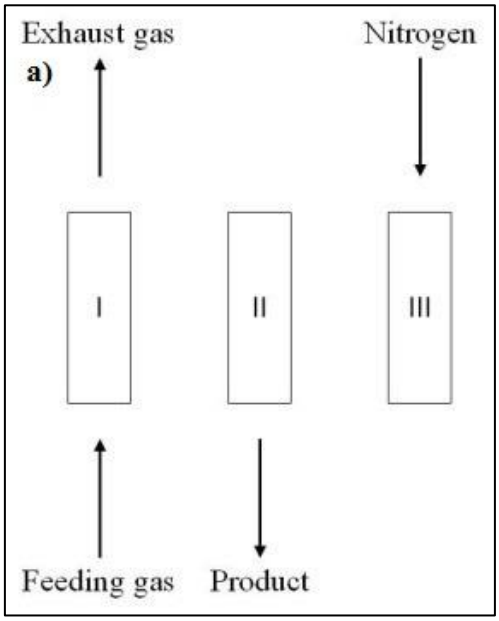

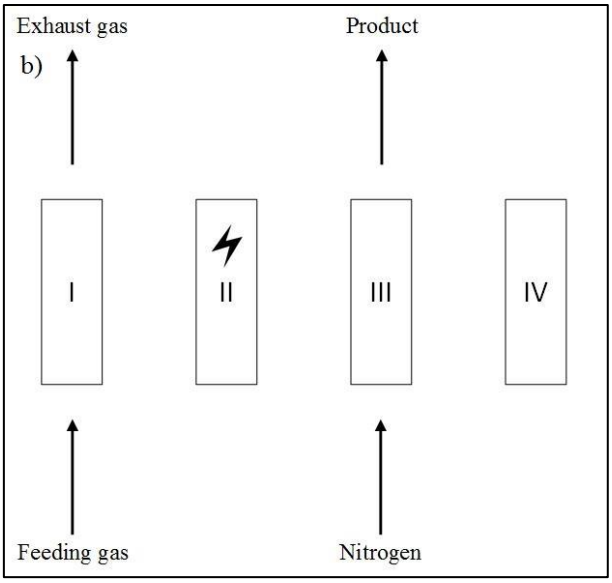

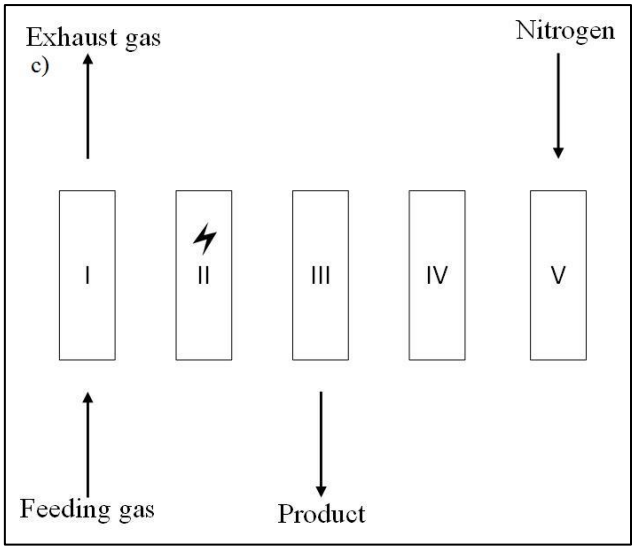

Fig.4: (a) 3-step VSA process: adsorption, vacuum desorption, and re-pressurization, (b), 4-step of ESA process: adsorption, electrification, purge and cooling (c) 5-step of VESA process: adsorption, electrification, vacuum desorption, cooling and re-pressurization

In the adsorption step, flue gas was fed to the adsorption column at a flowrate of 900 ml/min until the CO_2 concentration in the exhaust gas reached 5 %. In the succeeding desorption step, the column pressure was evacuated to an absolute pressure of 10, 20 and 30 kPa, respectively by extending different evacuation step times. In the re-pressurization step, N_2 was fed into the adsorption column until the pressure reached 103 kPa. In this cycle, the adsorption step was terminated when the exit concentration of CO_2 reached 5 %. Vacuum pressure at the end of the evacuation step was controlled to 10, 20 or 30 kPa, as desired. In the re-pressurisation step, N_2 gas was used to re-pressurize the monolith to 103 kPa before commencing the next cycle

3.4. ESA experiments

There were four steps in the cyclic ESA experiment: adsorption, electrification, N_2 purge and cooling, as shown in Fig.4b. The adsorption step was the same as that in VSA experiment described above. In the following electrification step, all valves were closed, and a constant voltage of 60.5 V was then applied for different electrification times of 30, 60, 90, 120, 150 and 180 s. In the following step of nitrogen purge, nitrogen gas co-currently purged the adsorption column for 150 s at a flowrate of 1200 ml/min (0.0617 m/s) and a pressure of 103 kPa. In the last step, the monolith was cooled by natural convection to room temperature for the next cyclic experiment.

3.5. VESA experiment

In contrast to the ESA process, in the VESA process, the N_2 purge was substituted with vacuum desorption. Following the electrification step, CO_2 adsorbed on the adsorbent or vaporised in the gas phase was evacuated from the system under vacuum pressure. The adsorption column was then re-pressurized with N_2 gas. The cooling step was the same as that in ESA. The operating parameters in ESA, VSA and VESA processes are shown in Table. 3.

Table. 3: Operating parameters in ESA, VSA and VESA adsorption-desorption cyclic experiments

ESA Process		
Electrification time (s)	Feeding time (s)	Desorption time(s)
30	168	40
60	178	40
90	183	40
120	188	40
150	190	40

180	191	40
VSA Process		
Vacuum pressure (kPa)	Feeding time (s)	Desorption time(s)
30	40	60
20	48	85
10	59	151
VESA Process		
Electrification time (s) - Vacuum pressure (kPa)	Feeding time (s)	Desorption time(s)
30-30	65	65
30-20	92	93
30-10	116	183
60-30	112	70
60-20	125	100
60-10	135	186
90-30	130	74
90-20	138	104
90-10	148	189

From our previous work [15], CO_2 product concentration was impacted significantly by electrification time. In this study, practical vacuum pressure (10 – 30 kPa) was employed to try to improve the separation performance of ESA process. For reducing energy consumption for CO_2 capture, thus, the electrification time for this experiment was chosen from 30 to 90 s. This combination of operating temperatures was found to provide satisfactory operation and did not exceed the temperature and pressure measurements of the system.

3.6. Calculation of the separation performance

3.6.1. Working capacity and selectivity

The working capacity of the adsorbent (WC) was calculated according to the isotherms of CO_2 on the adsorbent as the following equation[21], [22].

$$\mathrm{WC} = \mathrm{q}(\mathrm{T}_1, \mathrm{P}_1) - \mathrm{q}(\mathrm{T}_2, \mathrm{P}_2) \qquad (3)$$

Where $q(T_1, P_1)$ is the CO_2 adsorption amount at temperature T_1 and CO_2 partial pressure P_1 in the adsorption step, and $q(T_2, P_2)$ is that at temperature T_2 and regeneration pressure P_2 in the desorption step.

The selectivity (S) of CO_2 over N_2 can also be simply calculated as equation (4) [21, 23]:

$$S = \frac{q_{CO2}}{q_{N2}} \qquad (4)$$

Where, q_{CO2} is the equilibrium adsorption quantity of CO_2 and q_{N2} is that of N_2 at the same pressure and temperature.

3.6.2. CO_2 product purity and recovery

CO_2 purity and recovery in the rich CO_2 product can be calculated as:

$$Purity = \frac{\int_0^{t2} c_{CO2,out} v_{out} dt}{\int_0^{t2} v_{out} dt} \qquad (5)$$

$$Recovery = \frac{\int_0^{t2} c_{CO2,out} v_{out} dt}{\int_0^{t1} c_{CO2,in} v_{in} dt} \qquad (6)$$

Where, t_2 is the regeneration time (in VSA and VESA, it was desorption time, but in ESA, it was N_2 purge time, $c_{CO2,out}$ is an instantaneous CO_2 mole fraction in the desorption gas, v_{out} is an instantaneous flowrate of the desorption gas (sl/min); t_1 is the adsorption time, $C_{CO2,in}$ is an instantaneous CO_2 mole fraction in the feed gas and v_{in} is the feed gas flowrate (sl/min).

3.6.3. Power consumption in adsorption processes

In the VSA processes, the total energy consumption is from the feed blower and vacuum pump. This was calculated using the isentropic adiabatic power law by assuming a pump efficiency of 70% [23]:

$$Energy = \int_0^{t_{feed}} \frac{k}{k-1} \frac{Q_{feed} P_{feed}}{\eta} \left[\left(\frac{P_{feed}}{P_{atm}} \right)^{\frac{k-1}{k}} - 1 \right] \mathrm{d}t + \int_0^{t_{vac}} \frac{k}{k-1} \frac{Q_{vac} P_{vac}}{\eta} \left[\left(\frac{P_{atm}}{P_{vac}} \right)^{\frac{k-1}{k}} - 1 \right] \mathrm{d}t \quad (7)$$

where Q_{feed} and Q_{vac} represent instantaneous feed and CO_2 product flow-rate (m^3/s) respectively; P_{feed} and P_{vac} are the inlet and outlet pressures respectively (which may be different for adsorption and desorption steps (kPa)); t_{feed} and t_{vac} represent adsorption time and desorption time respectively (s); k is the ratio of heat capacities of the gas mixture at constant pressure and at constant volume (i.e. Cp/Cv, assumed to be 1.28 for CO_2 and 1.4 for N_2, here, k value was adjusted according to the compositions of the gas), and η is compressor/pump efficiency (0.7).

In the ESA process, vacuum energy consumption (the second part in equation 7) can be replaced by Joule heat (Q_{elc} − energy) used in a regeneration step:

$$Q_{elc} = \int_0^{t_{elc}} UI dt \quad (8)$$

Where U is the voltage applied to the hybrid monolith; I is the current intensity passing through the monolith, and t_{elc} is electrification time. Here, electrical energy was completely converted to heat energy for raising the temperature of the monolith.

Energy consumption in VESA processes includes the power used to generate joule heat (equation 8) and also that from compressor and vacuum pump (equation 7).

$$Energy = \int_0^{t_{feed}} \frac{k}{k-1} \frac{Q_{feed} P_{feed}}{\eta} \left[\left(\frac{P_{feed}}{P_{atm}} \right)^{\frac{k-1}{k}} - 1 \right] \mathrm{d}t + \int_0^{t_{vac}} \frac{k}{k-1} \frac{Q_{vac} P_{vac}}{\eta} \left[\left(\frac{P_{atm}}{P_{vac}} \right)^{\frac{k-1}{k}} - 1 \right] \mathrm{d}t + \int_0^{t_{elc}} UI dt \quad (9)$$

4. Results and Discussion

4.1. Comparison of the hybrid monolith and commercial AC monolith

Adsorption isotherms of CO_2 and N_2 at the same temperature of 293.15 K on the hybrid monolith and commercial activated carbon monolith [16] are shown in Fig. 5. Since CO_2 concentration in the feed gas is 15%, the partial pressure of CO_2 at atmospheric pressure is 15 kPa. As seen in Fig.5, the CO_2 loading on the hybrid monolith for pressures less than 20 kPa was higher than that on activated carbon. However, the hybrid monolith presented a more non-linear curvature so that a deeper vacuum pressure may be required to regenerate the adsorbent. In Fig.5b, the N_2 adsorption amounts on the zeolite were much lower than those on activated carbon, so that the zeolite monolith presented much higher selectivity of CO_2 over N_2 than the activated carbon monolith as shown in Fig.5c. The activated carbon monolith data were measured and reported in our previous work [16].

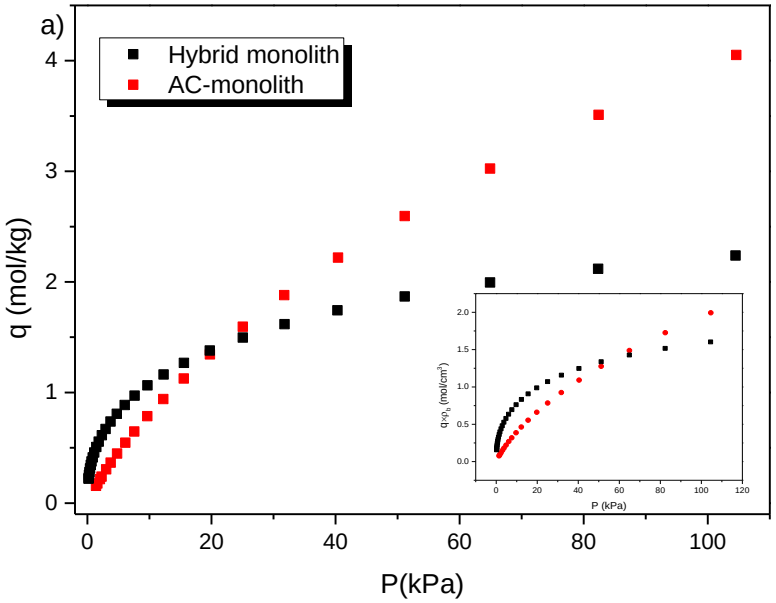
a)
Hybrid monolith
AC-monolith
q (mol/kg)
P(kPa)
0
1
2
3
4
0
20
40
60
80
100
P (kPa)

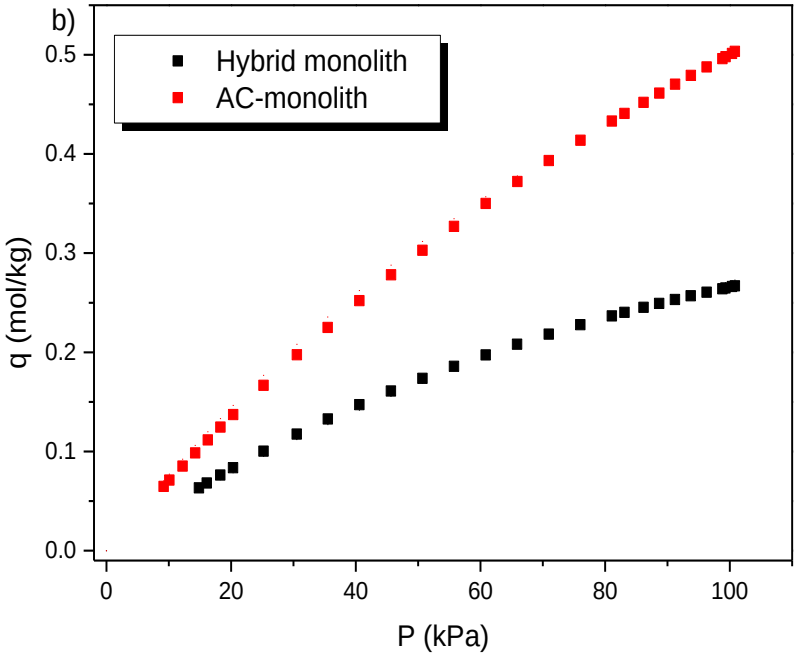
b)
Hybrid monolith
AC-monolith
q (mol/kg)
P (kPa)
0.0
0.1
0.2
0.3
0.4
0.5
0
20
40
60
80
100

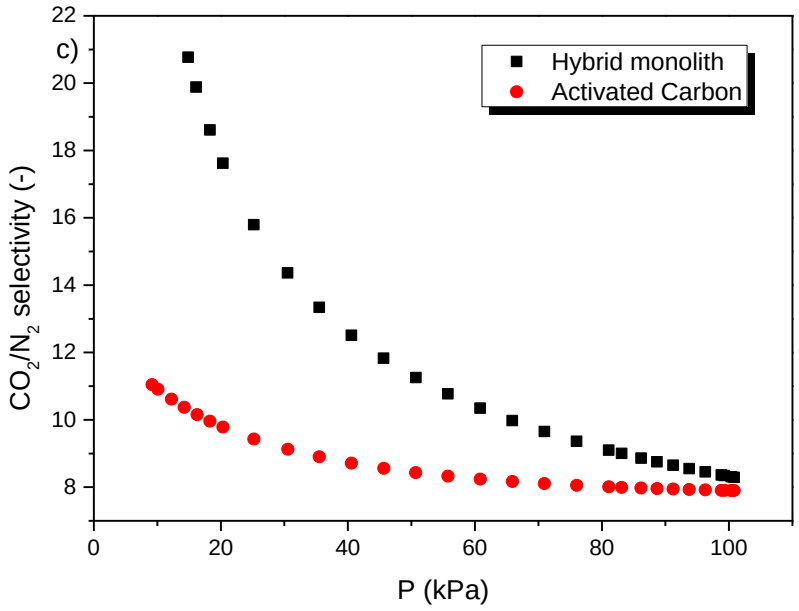

Fig.5: Adsorption isotherms of (a) CO_2, (b) N_2, and (c) selectivity of CO_2/ N_2 at the temperature of 293.15 K on the monoliths

It is seen clearly that the selectivity of CO_2/N_2 on the hybrid monolith rapidly drops as the pressure increases from 0 to 20 kPa and then gradually declines as the pressure is further increased. The introduction of zeolite H-ZSM-5 in the hybrid monolith improved the selectivity of CO_2/N_2 almost twice that of the commercial activated carbon in the pressure range below 20 kPa. Moreover, the wall density of hybrid monolith is higher than that of activated carbon monolith (989 kg/m^3) [18]. Thus, this improvement in adsorption capacity, selectivity, and wall density makes the hybrid monolith more appealing than an activated carbon-only monolith for CO_2 capture from flue gas.

Breakthrough experiments and simulation results on the hybrid monolith, and simulation data on the activated carbon monolith are shown in Fig. 6. The kinetic

coefficient (k_{LDF}) in the Linear Driving Force (LDF) model obtained by matching the breakthrough experiment data with simulation result was 0.12 s^{-1}, which was slightly higher than that of activated carbon monolith 0.1 s^{-1} [16], [24]. The simulation work of activated carbon monolith was based on our previous work at the same process conditions [16].

The higher selectivity and faster adsorption kinetics of the hybrid monolith resulted in a sharper breakthrough curve. Moreover, CO_2 adsorption quantity of hybrid monolith is higher than that of activated carbon for pressure lower than 20 kPa (shown in Figure 5a); and the wall density of hybrid monolith (1440 kg/m^3) is also higher than that of activated carbon monolith (989 kg/m^3). Thus, CO_2 adsorption capacity of hybrid monolith in the process is larger than that of activated monolith with the identical geometry shape, resulting in an extended breakthrough time.

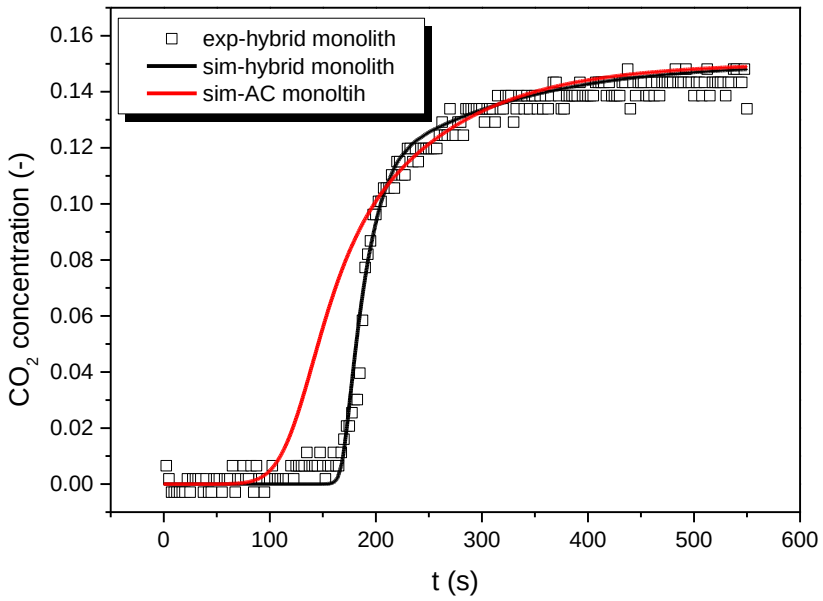

Fig. 6: Breakthrough data with the hybrid monolith and commercial AC; dot – experiment and lines - simulation

4.2. CO_2 working capacity of the hybrid monolith at various desorption temperatures and pressures

To understand the relative importance of vacuum and heating for the VESA process, we calculated the CO_2 working capacity for various combinations of regeneration temperature and desorption pressure. In this calculation, the adsorption capacity in the adsorption step – $q(T_1, P_1)$ (in equation 3) was calculated at the condition of 293 K and a pressure of 15 kPa. The adsorption capacity - $q(T_2, P_2)$ (in equation 3) at the end of desorption step was calculated as a function of regeneration temperature and pressure. In order to simplify the calculation, CO_2 concentration at the desorption condition of T_2 and P_2 was assumed to be 100%; however, it will be lower than 100% in reality. When T_2 is the same as T_1, the driving force for gas desorption is only ΔP (CO_2 partial pressure in the adsorption – CO_2 partial pressure at the end of desorption steps). By contrast, the driving force is only ΔT (the temperature difference between adsorption and desorption) when P_1 is equal to P_2. Contours of CO_2 working capacities for the hybrid monolith for different regeneration conditions are shown in Fig.7.

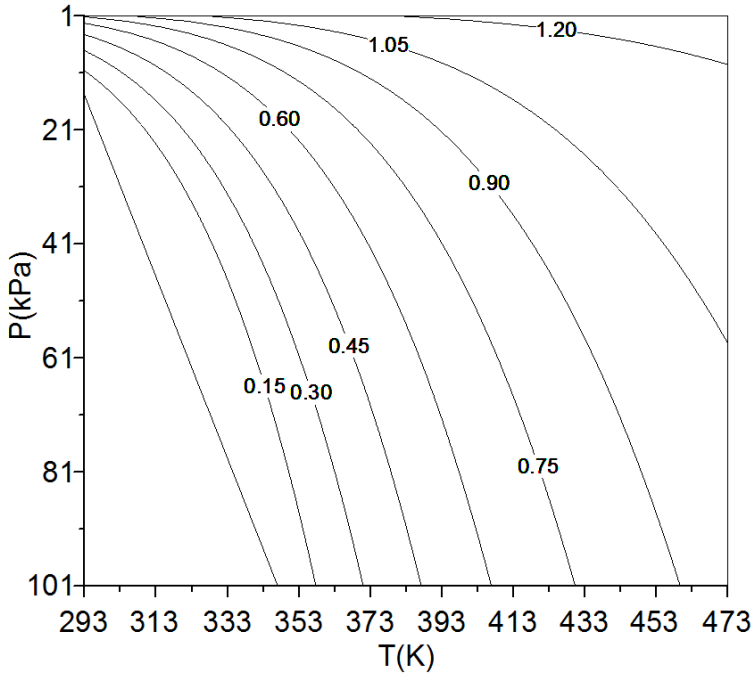

Fig.7: Contours of CO_2 working capacity (mmol/g) for the hybrid monolith as a function of regeneration temperature and regeneration pressure

From Fig.7, the working capacity increased as desorption temperatures increased and vacuum desorption pressure deepened, as expected. At a low regeneration temperature, vacuum pressure has a significant impact on the working capacity; for example, at a regeneration temperature of 358 K, the working capacity increased from 0.15 to 0.75 mol/kg as the desorption pressure changed from 101 to 14 kPa. By contrast, in the same pressure range, the working capacity only increased from 0.90 to 1.12 mol/kg at a regeneration temperature of 460 K. This is entirely in keeping with the shape of the isotherm as a function of temperature – at low temperatures, the CO_2 isotherm is strongly non-linear and large changes in capacity occur with small changes in pressure. At higher desorption temperatures, the isotherm slope is more linear and the change in loading with change in desorption pressure is more modest. The CO_2 equilibrium adsorption amount on this material is 1.2 mol/kg at 15 kPa and 293 K (Fig.2a). Thus, CO_2 can be almost completely desorbed at 473 K and a desorption

pressure of 10 kPa. At the temperature of 293 K, the working capacity was only 0.15 mol/kg at a desorption pressure (P_2) of 11 kPa, 0.30 mol/kg at 8 kPa and 0.45 mol/kg at 5 kPa. Therefore, vacuum-only desorption provides relatively low changes in CO_2 working capacity; and therefore vacuum alone for CO_2 desorption may be difficult.

4.3. Separation performance for VSA cyclic processes

As mentioned in section 3, the same adsorption steps were employed in VSA, ESA and VESA - only the desorption methods differed. From experimental observations, the VSA process reached steady state after running 3 to 4 cycles at which time the data were recorded. Although there are many experimental parameters which impact upon the performance of a VSA, the vacuum pressure is the key element which governs the performance since it provides the primary driving force for desorption. As a result, we focused on the desorption step to compare the competing processes.

The profiles of desorption flowrates and instantaneous CO_2 concentration during the vacuum desorption steps are shown in Fig.8a. The instantaneous flow rate and CO_2 concentrations for the three cases in which different end-of-step vacuum levels were used are shown in three colours (black, red, green) for the three-different end of step pressures (10, 20, 30 kPa, respectively). As expected, the three flow rate profiles are virtually identical since the end-of-step vacuum pressure was achieved by extending evacuation time, not increasing evacuation flow rate. The flow rate peaks at around 800 ml/min at the start of the evacuation step and then declines at deeper vacuum as expected.

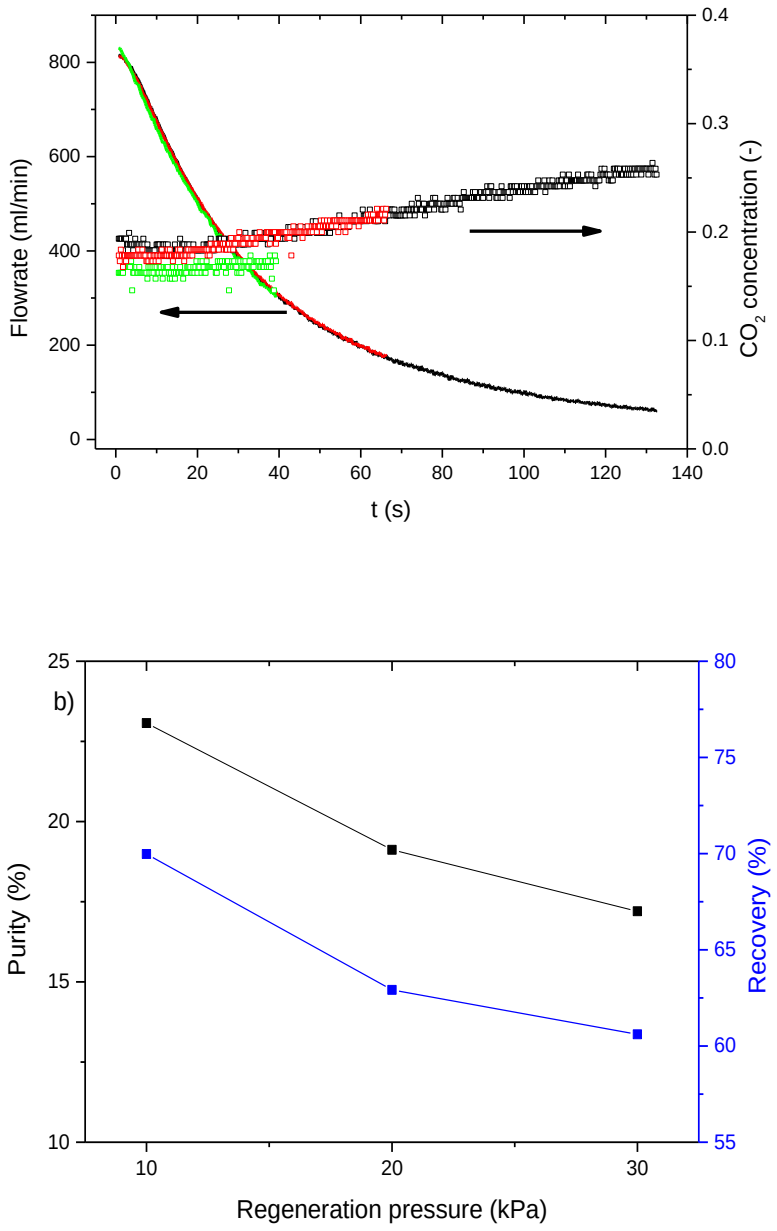

Fig.8: (a) profiles of instantaneous flowrate and CO_2 concentration during the desorption step at 10 kPa(black), 20 kPa(red), and 30 kPa(green) (b) average CO_2 purity and recovery as a function of final desorption pressure (kPa)

From Fig.8a, flowrates dropped rapidly in the initial desorption time and then gradually as desorption time continuously increased. In the desorption period of 65 s to 135 s (20 kPa to 10 kPa), only a small amount of gas was desorbed but the CO_2 concentration continuously increased, which corresponded to Fig.8b showing that

average CO_2 purity and recovery were improved from 19 to 23%. From Fig.8b, both CO_2 recovery and average purity increased as the desorption pressure deepened since the pressure driving force positively affected the VSA performance, which was consistent with CO_2 working capacity discussed above. The average CO_2 concentration declined from 23% to 17% and CO2 recovery from 70% to 61% as the desorption pressure changed from 10 kPa to 30 kPa. From this experiment, it was seen that vacuum pressure driving force alone was not good enough to obtain a high CO_2 purity product with this adsorbent.

4.4. Performance of ESA cyclic process

In this section, the effect of electrification time on the separation performance in a cyclic process was investigated and is discussed. Profiles of instantaneous flowrates and CO_2 concentration fraction with N_2 purge time are shown in Fig. 9a and 9b. As explained in our previous work [16], CO_2 gas was desorbed from the adsorbent since Joule heat of electrification lead to the rise of temperature, and the high temperature further resulted in a pressure increase in the adsorption column; the desorbed gas with a high pressure and a high CO_2 concentration was then suddenly released to the analyser at the beginning of the N_2 purge step so that the highest instantaneous flowrates and CO_2 concentration occurred as shown in Fig. 9a and 9b. The flowrate of desorption gas then dropped rapidly as the pressure in the adsorption column declined to atmospheric. Subsequently, the CO_2 concentrations and gas flowrates decreased gradually along with continuation of the N_2 purge. The rise of temperature in the adsorption column depends on Joule heat generated so that longer electrification time can result in more CO_2 desorption from the adsorbent, which corresponds to the experiment showing both CO_2 concentration fractions and flowrate peaks increased as electrification time increased. At the short electrification time such as 30 s, the

flowrate peak only appeared for a very short time before it decreased to the lowest value; the flowrate then increased until the N_2 purge run to 40 s; the flowrate slowly decreased as N_2 purge time further extended. The temperature difference caused by very short electrification time was not enough to completely desorb the CO_2. Thus, low CO_2 concentration gas appeared at the electrification time of 30 s. Since CO_2 loading in the column gradually decreased from the front to the end of the monolith, both flowrate and CO_2 concentration presented the same trend - increasing initially and then decreasing at short electrification time. The N_2 purge time was extended to 150 s to cool the monolith. From Fig. 9a and 9b, the most CO_2 desorbed by electrification was purged out in the first 40 s by N_2 gas. Therefore, the average CO_2 purity and recovery in the ESA cycle were calculated in the period of the first 40 s (as shown in Fig.9c).

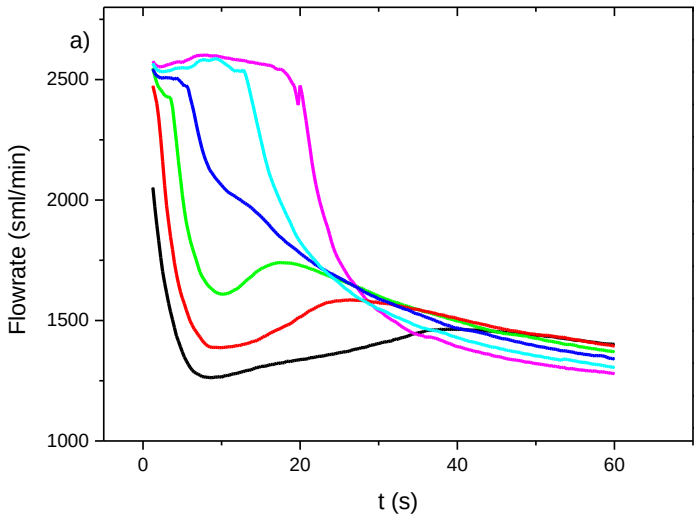

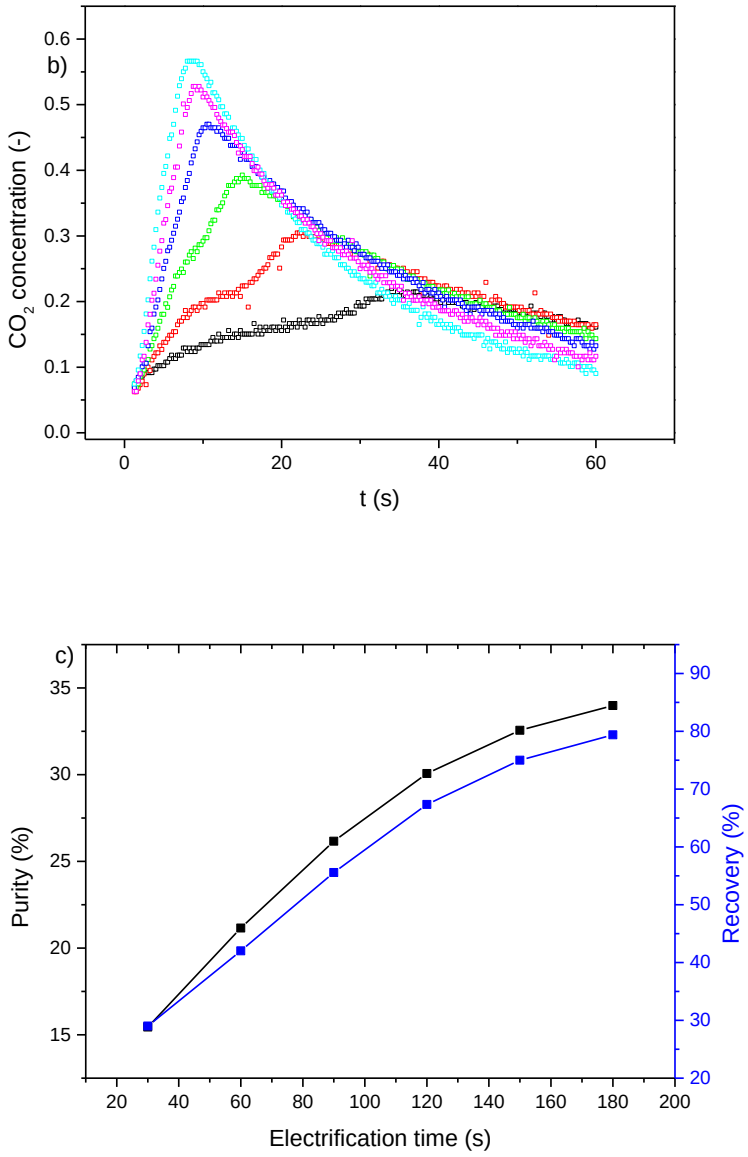

Fig.9: Profiles of (a) desorption flowrates (b) CO_2 concentrations with N_2 purge time at the electrification time of 30 s (black), 60 s (red), 90 s (green), 120 s (blue), 150 s (cyan) and 180 s (Magenta), and average CO_2 concentration and (c) recovery with electrification time

From Fig.9c, both average CO_2 concentration and recovery increased almost linearly from a CO_2 purity of 15% to 30% and a recovery of 29% to 67% as the electrification time increased from 30 to 120 s, and then slowed down as the electrification time further increased. Temperatures on the surface at different electrification time were

measured, and the corresponding ones in the middle of hybrid monolith were calculated from our previous work [16] (which is shown in table 4).

Tab. 4: Temperatures on the monolith at different electrification time

Electrification time (s)	30	60	90	120	150	180
Temperature on surface (K)	301	307	313	319	327	336
Temperature in middle (K)	322	347	374	401	436	474

As discussed above, extending electrification time benefits CO_2 desorption. However, the relative energy consumption would increase and longer cooling time may be required to reduce the high desorption temperature.

4.5. VESA performance

To improve the performance, VESA, as described earlier, was implemented. Thus, the vacuum desorption avoids CO_2 product gas dilution by inert gas. Fig.10 showed that instantaneous flowrates and CO_2 concentration fractions varied with vacuum desorption time at different electrification times. The vacuum pressure at the end of desorption was 30 kPa. Both flowrate peak and CO_2 fraction increased comparatively as electrification time increased. Compared with VSA shown in Fig.8a (only vacuum desorption at 295 K), both desorption flowrate and CO_2 concentration fraction in VESA improved significantly. The peak value of the flowrate at the short electrification time of 30 s reached 900 ml/min, but it was only 800 ml/min in VSA desorption. CO_2 fraction in VESA reached 0.28, but it was only 0.17 at the same vacuum pressure in VSA.

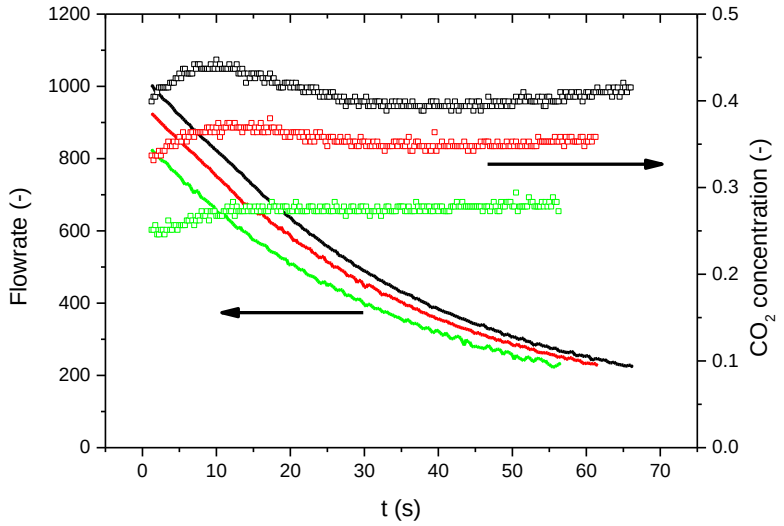

Fig.10: Instantaneous flowrates and CO_2 fractions with desorption time at the electrification time of 90 s (black), 60 s (red) and 30 s (green) for the end of desorption pressure of 30 kPa

Under a fixed electrification time of 90 s, instantaneous flowrate and CO_2 fraction with vacuum desorption time (the end of vacuum pressures reached 30, 20 and 10 kPa) were shown in Fig.11. Compared with vacuum desorption (Fig.8a), the flowrate peak value reached to around 1000 ml/min and CO_2 fraction was also improved.

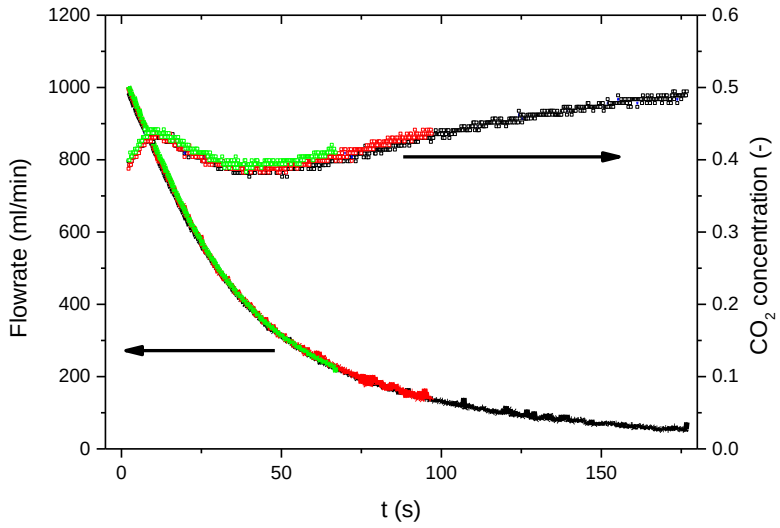

Fig.11: Instantaneous flowrate and CO_2 concentration with desorption time at the vacuum pressure of 10 kPa (black), 20 kPa (red) and 30 kPa (green) for the electrification time of 90 s

CO_2 product recovery and average CO_2 purity for the VESA process is summarised in Fig.12.

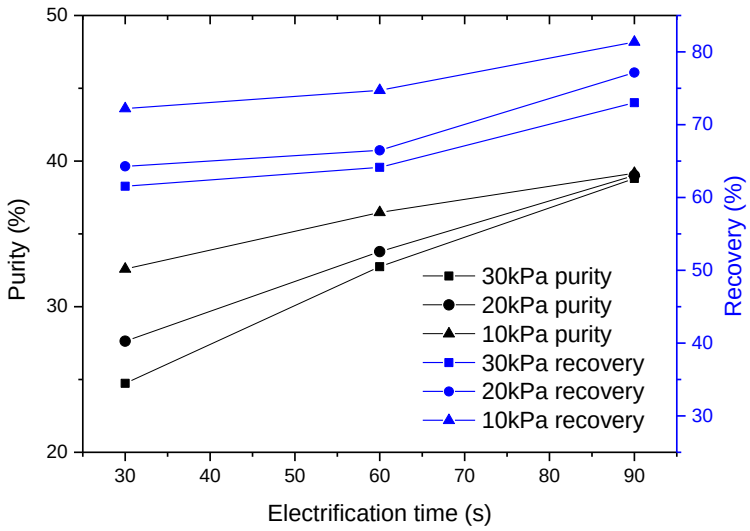

Fig.12: Average CO_2 purity and recovery at different pressures for electrification time of 90 s

In order to clearly present the advantages of VESA, average CO_2 purity and recovery for different running conditions are compared with those in VSA and ESA and the data are shown in table 5. Considering that more energy is consumed for long electrification time, the results with only shorter electrification time were shown here.

Tab. 5: Comparison of operating performance for VSA, ESA and VESA processes

	VSA			ESA			VESA		
Desorption condition	10 kPa	20 kPa	30 kPa	30 s	60 s	90 s	10 kPa + 30 s	20 kPa + 30 s	30 kPa + 30 s
Purity (%)	23	19	17	15	21	26	33	28	24
Recovery (%)	70	64	61	29	42	56	72	64	62

From Table 5, CO_2 purity and recovery were significantly improved with the VESA process. The CO_2 purity and recovery achieved 33% and 72% respectively at a vacuum desorption pressure of 10 kPa and electrification time of 30 s. It was obvious that the CO_2 purity was low (17 – 23%) in the VSA process even though the vacuum desorption pressure reached 10 kPa and CO_2 recovery (29 – 56%) was low at shorter electrification time in ESA.

4.6. Comparison of energy consumption for VSA, ESA and VESA

Energy consumption is always a key issue for the technology to be commercialised for CCS. CO_2 product mass generated, energy consumption in one cycle and specific energy in the different processes are summarised in Table 6. Because the adsorption step was run under an inlet pressure of 103 kPa, the energy consumed for compressing feed gas was ignored here.

Tab. 6: Energy consumption with different desorption processes

ESA process			
Electrification time (s)	kg.CO_2/cyc	Energy (J)	energy consumption (J/kg)
30	2.87×10^{-4}	873	3.04×10^{6}
60	4.41×10^{-4}	1956	4.43×10^{6}
90	6.00×10^{-4}	3188	5.31×10^{6}
120	7.45×10^{-4}	4525	6.08×10^{6}
150	8.52×10^{-4}	6037	7.08×10^{6}
180	9.32×10^{-4}	7821	8.39×10^{6}
VSA process			
Desorption pressure (kPa)	kg.CO_2/cyc	Energy (J)	energy consumption (J/kg)
30kPa	1.57×10^{-4}	38	2.45×10^{5}
20kPa	2.06×10^{-4}	57	2.80×10^{5}
10kPa	2.86×10^{-4}	96	3.34×10^{5}
VESA process			
Electrification time (s) - vacuum pressure (kPa)	kg.CO_2/cyc	Energy (J)	energy consumption (J/kg)
30-30	2.81×10^{-4}	914	3.25×10^{6}
30-20	3.51×10^{-4}	935	2.66×10^{6}
30-10	4.80×10^{-4}	980	2.04×10^{6}
60-30	4.24×10^{-4}	1998	4.71×10^{6}
60-20	4.93×10^{-4}	2022	4.10×10^{6}
60-10	6.16×10^{-4}	2065	3.35×10^{6}
90-30	5.50×10^{-4}	3231	5.87×10^{6}
90-20	6.26×10^{-4}	3254	5.20×10^{6}
90-10	7.15×10^{-4}	3292	4.61×10^{6}

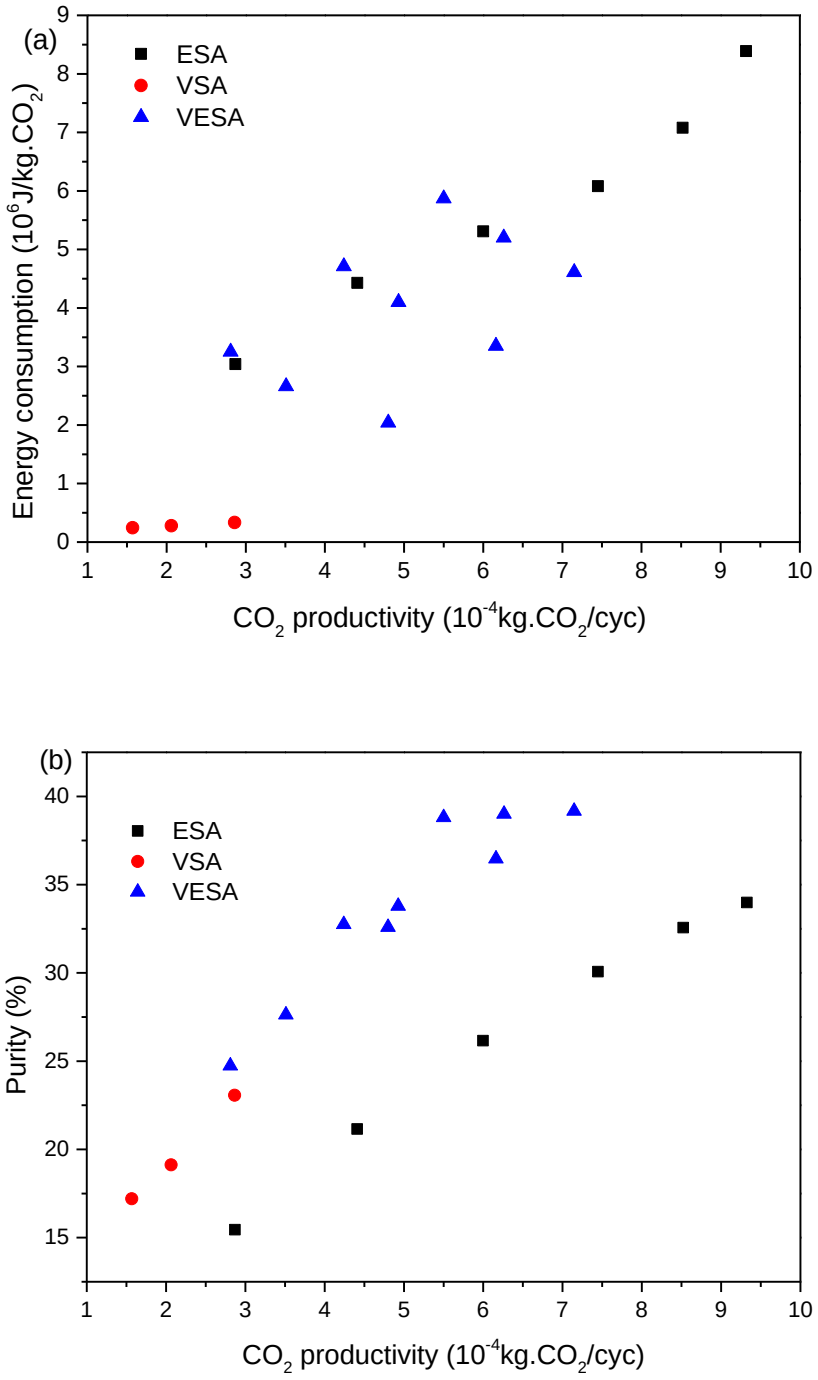

Fig.13: (a) Energy consumption for CO_2 capture and (b) CO2 purity for different cyclic processes

From Fig. 13a and 13b, the energy consumptions in the VSA-alone process is very low, compared with ESA and VESA processes. However, the CO_2 product purity

from the VSA desorption process is also very low and the maximum CO_2 productivity only reached 2.84×10^{-4} kg.CO_2/cyc (at 10 kPa) because the working capacity of this hybrid monolith was low at the running condition. At an electrification time of 30 s, the specific energy consumption in VESA at the desorption pressure of 30 kPa was slightly higher than that in ESA; but VESA showed its energy advantages at the desorption pressures of 10 and 20 kPa. However, compared with ESA and VESA, VSA presented its limitation in CO_2 product purification as shown in table 5 and Fig. 13b. VESA presented the highest CO_2 product purity at the same CO_2 productivity because it avoided product dilution by an inert gas. It is therefore apparent that slight vacuum can definitely improve the performance of the ESA-only system and this research provides motivation to further explore this concept. It may be beneficial to sequence the vacuum and electrification steps in an optimal manner to exploit the features of the adsorption isotherm.

Because of the small size of the adsorption rig developed in our lab, almost 25% of the electricity energy was spent within the contact resistance between the electrodes and the surface of the monolith, and some heat was also lost to the environment (large temperature difference between inside and surface of the monolith). The heat-electricity efficiency can be significantly improved with further development of the monolith adsorption system. Moreover, higher CO2 purity and recovery were obtained in other publications that studied TSA and ESA, [6], [15] . So, in order to reach higher CO2 purity and recovery, the cyclic process should be more sophisticated to ensure that the amount of inert gas inside the column is minimized.

Conclusions

The novel hybrid monolith combining zeolite ZSM-5 and activated carbon presented high CO_2 adsorption capacity and selectivity for CO_2 capture from the simulated flue gas streams, compared with commercial activated carbon monolith (MAST).

The CO_2 working capacity increased as regeneration temperature increased and desorption pressure deepened. The monolith seemed to be more sensitive to temperature so that high temperature regeneration would significantly improve the separation performance in the adsorption technologies.

In the VSA processes, we found that CO_2 purity in the desorbed gas flow was very low at a moderate desorption pressure of 10, 20 and 30 kPa. CO_2 purity and recovery in ESA increased as electrification time increased. There was not much change for the purity and recovery for short electrification time such as 30 s. Although longer electrification time could lead to more CO_2 recovery and higher purity product; the specific energy consumption for CO_2 capture also greatly increases, which is not desirable. VESA combining the advantages of VSA and ESA remarkably improved CO_2 capture performance from the simulated flue gas. CO_2 purity rose up 1.4 times compared to only VSA and 1.6 – 2.1 times compared to only ESA; the recovery improved slightly compared VSA and 2.1 to 2.5 times compared to ESA.

Both energy consumptions in ESA and VESA were much higher than those in VSA, so in the further work how to improve the efficient electrification process and how to develop the monolith which has a reasonable resistance and high adsorption characteristics will be important for the technology to be commercialised. This methodology can be certainly referenced in the separation of high valuable gases, or in some special area where energy consumption is not concerned.

Acknowledgements

We acknowledge the financial support of The University of Melbourne for this project as well as the funding support from Brown Coal Innovation Australia. We acknowledge the hybrid monolith supplied by our partners in the European Commission Framework 7 MATESA project. The research leading to these results has received funding from the European Union Seventh Framework Programme (FP7 2007 - 2013) under Grant Agreement 608534 (MATESA project). Jean-Jacques Theron from Corning, France is acknowledged for providing the materials used in this study.

References:

[1] C. T. Chou and C. Y. Chen, "Carbon dioxide recovery by vacuum swing adsorption," *Sep. Purif. Technol.*, vol. 39, no. 1–2 SPEC. ISS., pp. 51–65, 2004.

[2] J. Zhang, P. A. Webley, and P. Xiao, "Effect of process parameters on power requirements of vacuum swing adsorption technology for CO2 capture from flue gas," *Energy Convers. Manag.*, vol. 49, no. 2, pp. 346–356, 2008.

[3] J. Ling, A. Ntiamoah, P. Xiao, P. A. Webley, and Y. Zhai, "Effects of feed gas concentration, temperature and process parameters on vacuum swing adsorption performance for CO2 capture," *Chem. Eng. J.*, vol. 265, pp. 47–57, 2015.

[4] G. Li, P. Xiao, P. Webley, J. Zhang, R. Singh, and M. Marshall, "Capture of CO2 from high humidity flue gas by vacuum swing adsorption with zeolite 13X," *Adsorption*, vol. 14, no. 2–3, pp. 415–422, Jun. 2008.

[5] C. Shen, J. Yu, P. Li, C. A. Grande, and A. E. Rodrigues, "Capture of CO2 from flue gas by vacuum pressure swing adsorption using activated carbon beads," *Adsorption*, vol. 17, no. 1, pp. 179–188, 2011.

[6] L. Joss, M. Gazzani, and M. Mazzotti, "Rational design of temperature swing adsorption cycles for post-combustion CO2capture," *Chem. Eng. Sci.*, vol. 158, no. September 2016, pp. 381–394, 2017.

[7] L. Wang, Z. Liu, P. Li, J. Yu, and A. E. Rodrigues, "Experimental and modeling investigation on post-combustion carbon dioxide capture using zeolite 13X-APG by hybrid VTSA process," *Chem. Eng. J.*, vol. 197, pp. 151–

161, 2012.

[8] M. G. Plaza, S. García, F. Rubiera, J. J. Pis, and C. Pevida, “Post-combustion CO2 capture with a commercial activated carbon: Comparison of different regeneration strategies,” *Chem. Eng. J.*, vol. 163, no. 1–2, pp. 41–47, 2010.

[9] F. Su, C. Lu, A. J. Chung, and C. H. Liao, “CO2 capture with amine-loaded carbon nanotubes via a dual-column temperature/vacuum swing adsorption,” *Appl. Energy*, vol. 113, pp. 706–712, 2014.

[10] C. GRANDE and A. RODRIGUES, “Electric Swing Adsorption for CO2 removal from flue gases,” *Int. J. Greenh. Gas Control*, vol. 2, pp. 194–202, Nov. 2007.

[11] C. A. Grande, R. P. P. L. Ribeiro, and A. E. Rodrigues, “CO2 capture from NGCC power stations using Electric Swing Adsorption (ESA),” *Energy and Fuels*, vol. 23, no. 5, pp. 2797–2803, 2009.

[12] C. A. Grande, R. P. Ribeiro, and A. E. Rodrigues, “Challenges of electric swing adsorption for CO(2) capture,” *ChemSusChem*, vol. 3, no. 8, pp. 892–898, 2010.

[13] R. P. P. L. Ribeiro, C. A. Grande, and A. E. Rodrigues, “Electrothermal performance of an activated carbon honeycomb monolith,” *Chem. Eng. Res. Des.*, vol. 90, no. 11, pp. 2013–2022, 2012.

[14] R. P. P. L. Ribeiro, C. a. Grande, and a. E. Rodrigues, “Electric Swing Adsorption for Gas Separation and Purification: a Review,” *Sep. Sci. Technol.*, vol. 49, no. 13, pp. 1985–2002, 2014.

[15] S. Lillia, D. Bonalumi, C. Grande, and G. Manzolini, “A comprehensive modeling of the hybrid temperature electric swing adsorption process for CO_2capture,” *Int. J. Greenh. Gas Control*, vol. 74, no. October 2017, pp. 155–173, 2018.

[16] Q. Zhao, F. Wu, Y. He, P. Xiao, and P. A. Webley, “Impact of operating parameters on CO 2 capture using carbon monolith by Electrical Swing Adsorption technology (ESA),” *Chem. Eng. J.*, vol. 327, pp. 441–453, 2017.

[17] K. T. Chue, J. N. Kim, Y. J. Yoo, S. H. Cho, and R. T. Yang, “Comparison of Activated Carbon and Zeolite 13X for CO2 Recovery from Flue Gas by Pressure Swing Adsorption,” *Ind. Eng. Chem. Res.*, vol. 34, no. 2, pp. 591–598, 1995.

[18] R. P. P. L. Ribeiro, C. A. Grande, and A. E. Rodrigues, “Activated carbon honeycomb monolith – Zeolite 13X hybrid system to capture CO 2 from fl ue gases employing Electric Swing Adsorption,” *Chem. Eng. Sci.*, vol. 104, pp. 304–318, 2013.

[19] A. Masala *et al.*, “Conductive ZSM-5-Based Adsorbent for CO2 Capture: Active Phase vs Monolith,” *Ind. Eng. Chem. Res.*, vol. 56, no. 30, pp. 8485–8498, 2017.

[20] F. D. Yu, L. Luo, and G. Grevillot, “Electrothermal swing adsorption of

toluene on an activated carbon monolith. Experiments and parametric theoretical study," *Chem. Eng. Process. Process Intensif.*, vol. 46, no. 1, pp. 70–81, 2007.

[21] S. Cavenati, C. A. Grande, and A. E. Rodrigues, "Adsorption Equilibrium of Methane, Carbon Dioxide, and Nitrogen on Zeolite 13X at High Pressures," *J. Chem. Eng. Data*, vol. 49, no. 4, pp. 1095–1101, Jul. 2004.

[22] Z. Liang, M. Marshall, and A. L. Chaffee, "CO2 adsorption-based separation by metal organic framework (Cu-BTC) versus zeolite (13X)," *Energy and Fuels*, vol. 23, no. 5, pp. 2785–2789, 2009.

[23] A. Ntiamoah, J. Ling, P. Xiao, P. A. Webley, and Y. Zhai, "CO2 capture by vacuum swing adsorption: role of multiple pressure equalization steps," *Adsorption*, vol. 21, no. 6–7, pp. 509–522, 2015.

[24] Q. Zhao *et al.*, "Synthesis of a novel hybrid adsorbent which combines activated carbon and zeolite NaUSY for CO 2 capture by Electric Swing Adsorption (ESA)," *Chem. Eng. J.*, 2017.